

# An Order–Disorder Ferroelectric Host–Guest Inclusion Compound\*\*

Yi Zhang, Heng-Yun Ye, Da-Wei Fu, and Ren-Gen Xiong\*

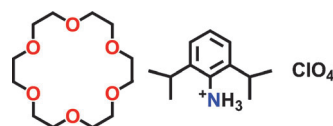
**Abstract:** The host–guest complex [(DIPA)([18]crown-6)]-(ClO<sub>4</sub>) (**1**; DIPA = 2,6-diisopropylanilinium) was constructed and found to undergo a sequence of phase transitions (Ibam–Pbcn–Pna2<sub>1</sub>) at  $T_1=278$  K and  $T_2=132$  K, respectively. Systematic characterizations, such as differential scanning calorimetry, heat capacity, temperature-dependent dielectric constant, and *P*–*E* hysteresis loop, reveal that the centrosymmetric-to-polar phase transition at  $T_2$  is a paraelectric-to-ferroelectric transition. The symmetry breaking was also confirmed by temperature-dependent second-harmonic generation effect and X-ray powder diffraction. The ferroelectric mechanism is attributable to the linear motion of the perchlorate counterions accompanied by the order–disorder transition of the [18]crown-6 molecules and the anions.

Molecular ferroelectrics have recently attracted much attention from researchers in the fields of chemistry, physics, and materials science.<sup>[1–6]</sup> Their high performance is comparable to that of pure inorganic ferroelectrics, such as large spontaneous polarization and high Curie temperature,<sup>[4]</sup> as well as new ferroelectric physics, such as charge-transfer along  $\pi$ – $\pi$ -stacked supramolecular networks of electron donors and acceptors leading to spontaneous polarization.<sup>[7]</sup> In contrast to inorganic ferroelectric oxide compounds, molecular ferroelectrics have advantages in many aspects, such as light weight, nontoxicity, easy processability, structural tunability, and multifunctionality. A key problem in developing ferroelectrics is to construct new types of compounds, which needs deep understanding of the origin of ferroelectricity. Up to now, in molecule-based ferroelectrics, the most commonly employed mechanism is of order–disorder type. One example is hydrogen-bonded organic ferroelectrics such as [(dabaco)ReO<sub>4</sub>] in which the order–disorder transition of the protons induce the occurrence of polarization.<sup>[1]</sup> Other examples include order–disorder-type ferroelectrics, and especially organic salt-type, with relatively larger organic and/or inorganic groups.<sup>[2–6]</sup>

Host–guest compounds are a very promising class of molecular ferroelectrics, for example, [18]crown-6-based compounds.<sup>[5,6]</sup> Generally, the [18]crown-6 molecule acts as a host of which the six O atoms afford lone-pair electrons to anchor the guest ammonium cation. The guest ion may

undergo rotational/hopping motion like a molecular rotator or local wobbling/twisting motion, producing an order–disorder type ferroelectric phase transition. This has been evidenced in the first molecular pendulum-like ferroelectrics [(C<sub>7</sub>H<sub>10</sub>NO)([18]crown-6)][BF<sub>4</sub>] and [(C<sub>7</sub>H<sub>10</sub>NO)([18]crown-6)][ReO<sub>4</sub>] (C<sub>7</sub>H<sub>10</sub>NO = 4-methoxyanilinium cation).<sup>[6]</sup> The origin of their ferroelectricity is due to the order–disorder transition of the pendulum-like motions of the guest 4-methoxyanilinium cation.

Herein, we report a new host–guest ferroelectric compound [(DIPA)([18]crown-6)](ClO<sub>4</sub>) (**1**; DIPA = 2,6-diisopropylanilinium; Scheme 1). Structurally, compound **1** is



**Scheme 1.** The structural formula of compound **1**.

analogous to [(C<sub>7</sub>H<sub>10</sub>NO)([18]crown-6)][BF<sub>4</sub>].<sup>[6a]</sup> However, it shows a different phase transition behavior and the origin of ferroelectricity is found not from motional changes of the DIPA guest cation but from the order–disorder transition of the [18]crown-6 host molecule and perchlorate counterion.

Crystals of **1** were obtained by slow evaporation of an acetone solution containing 2,6-diisopropylaniline, [18]crown-6, and HClO<sub>4</sub> at room temperature. Phase purity of **1** was confirmed by powder X-ray diffraction and IR analysis (Supporting Information, Figures S1 and S2 a).

The phase transition behavior of **1** was firstly evidenced by heat capacity (*C<sub>p</sub>*) and differential scanning calorimetry (DSC; Figure 1). The DSC curves clearly show two phase transitions at 278 K ( $T_1$ ) and 132 K ( $T_2$ ), respectively. The phase above  $T_1$  is designated as the high-temperature phase (HTP), the phase between  $T_1$  and  $T_2$  as the intermediate-

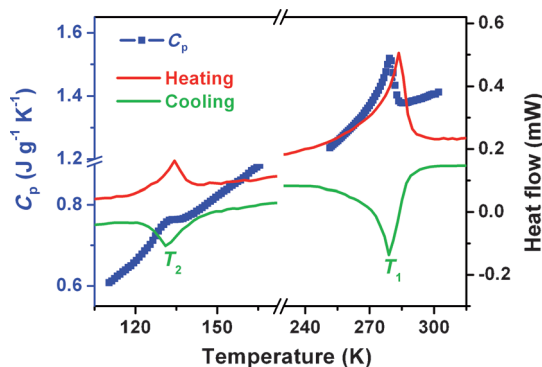


**Figure 1.** Heat capacity and DSC measurements of **1**.

[\*] Dr. Y. Zhang, Dr. H.-Y. Ye, Dr. D.-W. Fu, Prof. R.-G. Xiong  
Ordered Matter Science Research Center  
Southeast University, Nanjing 211189 (P.R. China)  
E-mail: xionggr@seu.edu.cn

[\*\*] This work was supported by the Project 973 2014CB848800, the National Natural Science Foundation of China (21290172, 21101025 and 91222101).

Supporting information for this article is available on the WWW under <http://dx.doi.org/10.1002/anie.201307690>.

temperature phase (ITP), and the phase below  $T_2$  as the low-temperature phase (LTP). The broad peaks and the narrow temperature hysteresis (2 K) of the thermal anomalies indicate that both phase transitions are of second-order type. Entropy changes ( $\Delta S$ ) accompanying the phase transitions at around  $T_1$  and  $T_2$  are about  $5.216 \text{ J mol}^{-1} \text{ K}^{-1}$  and  $2.585 \text{ J mol}^{-1} \text{ K}^{-1}$ , respectively. According to the Boltzmann equation,  $\Delta S = R \ln N$ , where  $R$  is the gas constant and  $N$  is the ratio of the number of respective geometrically distinguishable orientations, the values of  $N(T_1)$  and  $N(T_2)$  are calculated as 1.87 and 1.36, respectively, indicating the disorder–order feature of the two phase transitions. The  $C_p$  measurement of **1** was taken in two temperature ranges around the phase transition points  $T_1$  and  $T_2$ . The  $C_p$  curves also obviously show two thermal anomalies at around 278 K and 132 K, matching well with the DSC measurement.

Variable-temperature X-ray diffraction analysis of **1** confirms it undergoes two sequential structural phase transitions with space group  $Ibam$  in HTP,  $Pbcn$  in ITP, and  $Pna2_1$  in LTP.<sup>[8]</sup> At room temperature, the crystal structure consists of host [18]crown-6 molecules and guest DIPA cations with  $\text{ClO}_4^-$  as counterpart anions (Figure 2a). The DIPA cation is situated in the cavity of the [18]crown-6 molecule by N–H $\cdots$ O hydrogen-bonding interactions. The H-bonded DIPA $\cdots$ [18]crown-6 moiety is located at the mirror site. The intramolecular mirror plane of the DIPA cation is superimposed with the crystallographic mirror plane, whereas the mirror symmetry of the [18]crown-6 molecule is satisfied by the orientational disorder. Different from the common 2D symmetrical disk-shaped structure,<sup>[9]</sup> the structure of the [18]crown-6 molecule is boat-shaped owing to the steric hindrance between the skeleton of the [18]crown-6 molecule and the two isopropyl groups of the DIPA cation. The alternated DIPA cations and [18]crown-6 molecules form columns along the  $b$ -axis. The tetrahedral  $\text{ClO}_4^-$  is disordered over two orientations; the Cl atom lies on the twofold rotation axis along the  $b$ -axis direction. The packing view of **1** at 293 K along the  $b$ -axis is illustrated in the Supporting Information, Figure S3.

At 173 K, the ITP remains centrosymmetric.<sup>[8]</sup> A common origin and axial directions similar to those of the HTP was chosen. The asymmetric unit contains one DIPA cation, one [18]crown-6 molecule, and two half-perchlorate anions, as shown in Figure 2b. The [18]crown-6 molecule becomes ordered and loses the mirror symmetry. The  $\text{ClO}_4^-$  anions remain on the special position with twofold axis symmetry. One  $\text{ClO}_4^-$  anions becomes ordered, and the other remains disordered over two staggered orientations with a common O–Cl bond. This bond is superimposed on the crystallographic twofold axis. Except the ordering, the crystal structure is similar to the RTP (Supporting Information, Figures S3 and S4).

At 93 K, the LTP assumes a polar space group. The relationship between the two cells at 93 and 173 K is  $\mathbf{a}^{93\text{K}} \approx \mathbf{c}^{173\text{K}}$ ,  $\mathbf{b}^{93\text{K}} \approx \mathbf{b}^{173\text{K}}$ , and  $\mathbf{c}^{93\text{K}} \approx \mathbf{a}^{173\text{K}}$ . The structure is refined with a racemic twinning model with the Flack parameter<sup>[10]</sup> of 0.65(4). For ferroelectric crystals, the domain structure is identical with the twinning structure.<sup>[11]</sup> The refinement reveals the LTP consists of  $180^\circ$  ferroelectric domains, the

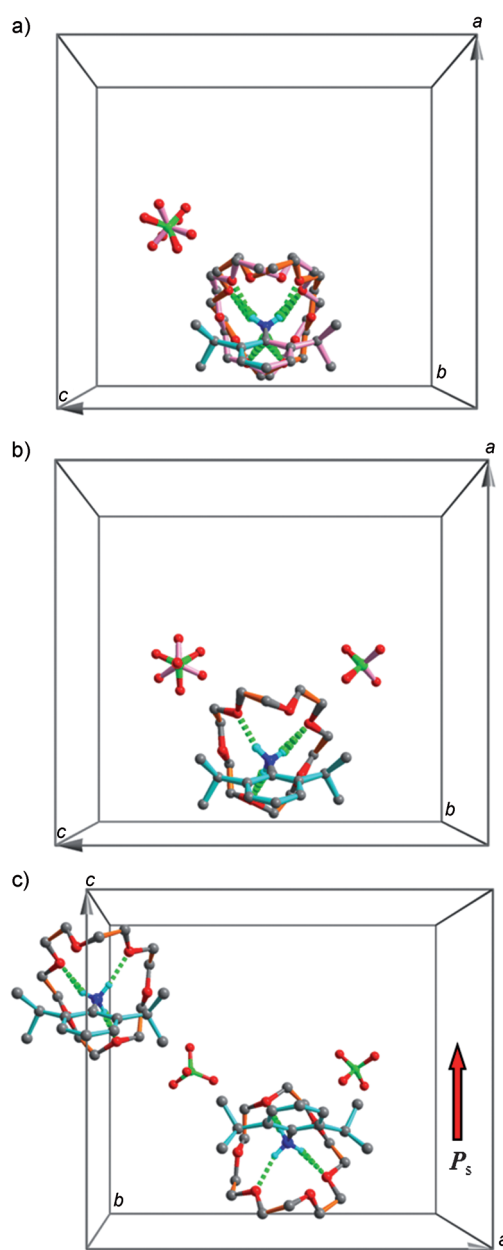


**Figure 2.** Asymmetric units of **1** in a) the high-temperature phase (HTP, 293 K), b) the intermediate-temperature phase (ITP, 173 K), and c) the low-temperature phase (LTP, 93 K). C gray, H pale blue, N dark blue, O red, Cl green. The parts with pink-colored bonds are generated by symmetry operation in (a) and (b). H atoms bonded to the C atoms are omitted for clarity. The red arrow in (c) indicates the direction of spontaneous polarization ( $P_s$ ).

fraction of the domain with present absolute structure being 0.35(4), that of the corresponding inverted structure being 0.65(4). The presence of ferroelectric domain structure is the result of minimizing the free energy of the ferroelectric crystal.<sup>[12]</sup> The asymmetric unit contains two molecular units. The obvious structural change is the further ordering of the disordered  $\text{ClO}_4^-$  anion in the ITP. The ordering leads to the single orientation of this anion (Figure 2c). In the ITP, the crystallographic twofold axis symmetry of this  $\text{ClO}_4^-$  anion along the  $b$ -axis is satisfied by the twofold orientational

disorder (Figure 2b), while in the LTP the intra-anionic twofold axis is not superimposed with crystallographic twofold axis, and the crystallographic twofold axis symmetry along the *b*-axis is broken. The check of additional symmetry of the crystal structure with PLATON<sup>[13]</sup> reveals that the structure has pseudo center of symmetry. That means that except for the ordering of the ClO<sub>4</sub><sup>-</sup> anions, the ferroelectric phase at 93 K just shows small structural change from that of paraelectric phase at 173 K. It appears that the order-disorder transition of the [18]crown-6 and/or ClO<sub>4</sub><sup>-</sup> anions play an important role in the phase transitions. The difference between the three temperature structures can be seen in the Supporting Information, Figures S3–S5.

The space group of **1** changes from *Ibam* to *Pbcn* to *Pna2<sub>1</sub>* during the two-phase-transition process. In the HTP, **1** adopts a centrosymmetric space group *Ibam* belonging to a nonpolar point group *D<sub>2h</sub>*. The ITP changes into a lower symmetric space group *Pbcn*. In this phase transition, symmetry breaking does not occur and the symmetric elements remain unchanged. In the LTP, **1** still belongs to an orthorhombic crystal system but with a noncentrosymmetric space group *Pna2<sub>1</sub>* (polar point group *C<sub>2v</sub>*). Symmetry breaking occurs with an Aizu notation of *mmmFmm2*. The eight symmetric elements (*E*, *C<sub>2</sub>*, *C<sub>2</sub>'*, *C<sub>2</sub>''*, *i*, *σ<sub>h</sub>*, *σ<sub>v</sub>*, *σ<sub>v</sub>'*) in the paraelectric phase (ITP) are halved into four (*E*, *C<sub>2</sub>*, *σ<sub>v</sub>*, *σ<sub>v</sub>'*) in the ferroelectric phase (LTP), a typical second-order phase transition feature according to Landau phase transition theory.<sup>[14]</sup> According to the Curie symmetry principle, the space group in the ferroelectric phase is a subgroup of the one in the paraelectric phase (primary phase), that is, *Pna2<sub>1</sub>* is a subgroup of *Pbcn* whose maximal nonisomorphic subgroups include *Pna2<sub>1</sub>*, *Pnc2*, *Pca2<sub>1</sub>*, *P2<sub>1</sub>2<sub>1</sub>2*, *P2<sub>1</sub>/c*, and *P2/c*, while the nonisomorphic subgroups of *Ibam* also cover *Pbcn*. Therefore, *Pbcn* probably can be taken as a modulated commensurate phase.

The second harmonic generation (SHG) effect in crystals is an effective way to test symmetry-breaking during phase transitions because noncentrosymmetric solids are SHG-active. Therefore, we performed SHG measurement to confirm the centrosymmetric-to-noncentrosymmetric phase transition.<sup>[15]</sup> As shown in Figure 3, **1** begins to be SHG-active and shows a clear peak at 532 nm (frequency doubling) below 132 K, corresponding to the phase transition from a centro-

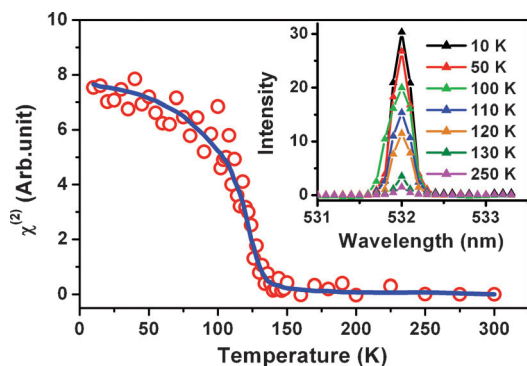


**Figure 3.** Temperature dependence of the second-order nonlinear effective coefficient of **1**. Inset: Intensity of SHG as a function of wavelength at different temperatures.

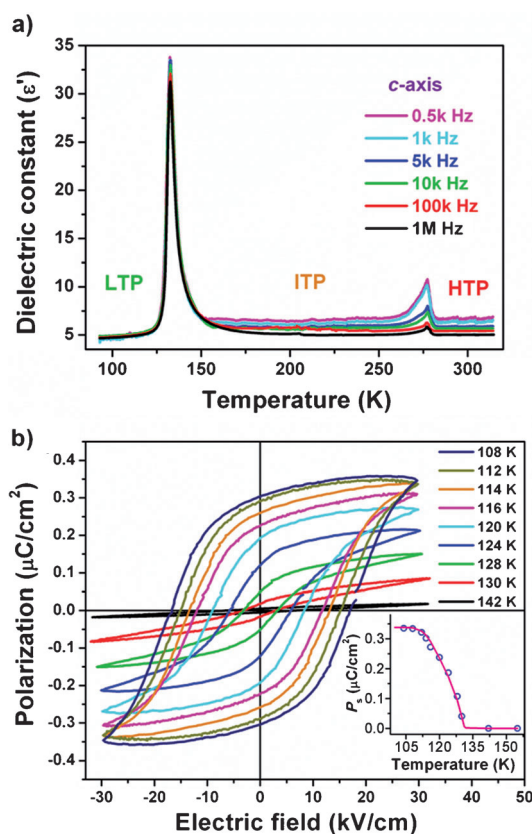


**Figure 4.** a) Dielectric constants of **1** measured along the *c*-axis with frequencies of 500 Hz to 1 MHz. (b) Electric hysteresis loop of **1** measured at various temperatures. Inset:  $P_s$  versus  $T$  curve of **1**.

symmetric structure (*Pbcn*) above 132 K to a noncentrosymmetric one (*Pna2<sub>1</sub>*) below 132 K. Above 132 K, no SHG signal is observed, indicating the ITP and HTP are centrosymmetric, consistent with the space groups *Ibam* and *Pbcn*. The value of the temperature-dependent effective second-order nonlinear optic susceptibility  $\chi^{(2)}$  behaves like spontaneous polarization ( $P_s$ ; inset of Figure 4b), consistent with the Landau relationship  $\chi^{(2)} = 6\epsilon_0\beta P_s$ , where  $\beta$  is almost independent of the temperature. Both the variations of  $P_s$  and  $\chi^{(2)}$  in the vicinity of  $T_2$  are continuous, revealing a second-order phase transition.<sup>[16]</sup>

The temperature dependence of the real part of the complex relative dielectric permittivity ( $\epsilon'$ ) of **1** was measured along the three crystallographic axes on the single-crystal sample and on powdered sample with various frequencies (Figure 4a; Supporting Information, Figure S6). The crystal faces of the LTP are selected in the measurement. As shown in Figure 4a, the temperature dependent dielectric permittivity along the *c*-axis also exhibits two dielectric anomalies at around 278 and 132 K upon cooling, consistent with the results of  $C_p$  and DSC measurements. At around 278 K, the dielectric constants only show small anomalies from about 5 to 5.6. In contrast to this, large dielectric anomalies were observed at around 132 K with the peak value of about 35, corresponding to an enhancement of five times, which is the characteristic feature of paraelectric–ferroelectric phase transitions. The reciprocal of dielectric constants around the

ferroelectric phase transition point can be well fitted with the Curie–Weiss law,  $\varepsilon = C/(T - T_0)$ , where  $C$  is the Curie–Weiss constant and  $T_0$  is the Curie temperature. The fitted parameters at different frequencies indicate that the value of  $T_0$  decreases with the increase of frequency and is almost equal to  $T_2$  at 1 MHz, suggesting the phase transition is of a second-order type (Supporting Information, Table S1). The value of  $C_{\text{para}}$  and  $C_{\text{ferro}}$  decreases with increasing frequency. The ratio of  $C_{\text{para}}$  to  $C_{\text{ferro}}$  is in the range of 2.69–2.41 and smaller than 4, also indicating a second-order phase transition.

Polarization as a function of the applied electric field of **1** was measured with  $E//c$  at different temperatures in a cooling run. The  $P$ – $E$  loop is nearly a straight line without obvious hysteresis above 130 K. At 130 K, just below  $T_2$ ,  $P_s$  occurs and the characteristic dielectric hysteresis loop appears. Upon further cooling,  $P_s$  increases gradually and reaches saturation at about 108 K with a saturation polarization of  $0.35 \mu\text{C cm}^{-2}$ . The inset of Figure 4b represents the temperature dependence of  $P_s$  deduced from the  $P$ – $E$  hysteresis loops. Pyroelectric measurement is also an effective method to characterize the temperature dependence of  $P_s$ . Figure S7 clearly shows that above  $T_2$ ,  $P_s$  is zero, while below  $T_2$ , it increases gradually and reaches an maximum value of  $0.42 \mu\text{C cm}^{-2}$ . The behavior of the temperature-dependent  $P_s$  is consistent with that deduced from  $P$ – $E$  hysteresis loop measurement (inset of Figure 4b). According to Landau phase transition theory,  $P_s$  can be calculated by the formula  $P_s = (2\varepsilon_0 C \Delta S)^{1/2}$ , where  $P_s$ ,  $\varepsilon_0$ ,  $\Delta S$ , and  $C$  stand for spontaneous polarization, vacuum permittivity, entropy change, and Curie–Weiss constant, respectively. If  $\Delta S = 2.585 \text{ J mol}^{-1} \text{ K}^{-1}$  and  $C = 150.4 \text{ K}$  at 500 Hz are put into the equation,  $P_s$  is estimated to be  $0.398 \mu\text{C cm}^{-2}$ , which is fairly consistent with the experimental result. Meanwhile, with the point charge model (Supporting Information, Figure S8), the estimated value ( $0.1 \mu\text{C cm}^{-2}$ ) is in the same order of magnitude as that from the experiment (Supporting Information, Table S2).

In summary, this work has demonstrated that the host–guest compound [(DIPA)([18]crown-6)](ClO<sub>4</sub>) undergoes a paraelectric-to-ferroelectric phase transition at 132 K, characterized by X-ray diffraction measurement, thermal analysis, and dielectric and second harmonic generation experiments. Origin of the ferroelectricity is attributable to the synergistic order–disorder transitions of the host [18]crown-6 molecule and perchlorate counterion rather than the rotation of the guest DIPA cation, which is different from the known mechanism in other host–guest ferroelectrics.<sup>[6]</sup> It points out a new way to explore and design novel molecule-based ferroelectric compounds.

### Experimental Section

All of the reagents and solvents in the synthesis were of reagent grade and used without further purification. Evaporation of a acetone solution (50 mL) containing 2,6-diisopropylaniline (1.77 g, 0.01 mol), [18]crown-6 (2.64 g, 0.01 mol), and HClO<sub>4</sub> (1.4 g, 0.01 mol) results in the formation of **1** as colorless crystals. IR:  $\tilde{\nu} = 3128$  (vs, NH<sub>3</sub><sup>+</sup>), 1467 (s, C=C), 1109 cm<sup>-1</sup> (vs, ClO<sub>4</sub><sup>-</sup>).

Variable-temperature X-ray diffraction analysis was carried out on **1** using a Rigaku CCD diffractometer with MoK<sub>α</sub> radiation ( $\lambda =$

0.71073 Å). Data collection, cell refinement, and data reduction was performed using Rigaku CrystalClear 1.3.5. The structure of **1** was solved by direct methods and refined by the full-matrix method based on  $F^2$  using the SHELXL97 software package. All non-hydrogen atoms were refined anisotropically and the positions of all hydrogen atoms were generated geometrically. CCDC 891944, 891945, 891946 for **1** contain the supplementary crystallographic data for this paper. These data can be obtained free of charge from The Cambridge Crystallographic Data Centre via [www.ccdc.cam.ac.uk/data\\_request/cif](http://www.ccdc.cam.ac.uk/data_request/cif).

X-ray powder diffraction was measured on a Rigaku DMX/2000 X-ray diffraction instrument. Specific heat analyses were carried out on a Quantum Design PPMS. Differential scanning calorimetry experiments were performed on a NETZSCH DSC 200 F3 under a nitrogen atmosphere in aluminum crucibles with the heating and cooling rate of 10 K min<sup>-1</sup>. For dielectric, ferroelectric, and pyroelectric measurements, the samples were made with single crystals cut into the form of thin plates perpendicular to the crystal axes. Silver conductive paste deposited on the plate surfaces was used as the electrodes. Complex dielectric permittivity was measured with an Agilent 4284A impedance analyser at the frequency range from 20 Hz to 1 MHz with an applied electric field of 0.5 V. Dielectric hysteresis loops were recorded on a Radiant Precision Premier II. Pyroelectric properties were measured with an electrometer/high resistance meter (Keithley 6517B). For SHG experiments, an unexpanded laser beam with low divergence (pulsed Nd:YAG at a wavelength of 1064 nm, 5 ns pulse duration, 1.6 MW peak power, 10 Hz repetition rate) was used. The instrument model is FLS 920, Edinburgh Instruments and the low temperature system is 10–325 K, DE 202, while the laser is Vibrant 355 II, OPOTEK. The numerical values of the nonlinear optical coefficients for SHG were determined by comparison with a KDP reference.

Received: September 1, 2013

Revised: December 3, 2013

Published online: February 4, 2014

**Keywords:** dielectric constant · ferroelectrics · host–guest compounds · order–disorder · phase transitions

- [1] a) A. Katrusiak, M. Szafranski, *Phys. Rev. Lett.* **1999**, *82*, 576–579; b) A. Katrusiak, M. Szafranski, G. J. McIntyre, *Phys. Rev. Lett.* **2002**, *89*, 215507; c) S. Horiuchi, Y. Tokura, *Nat. Mater.* **2008**, *7*, 357–366.
- [2] a) S. Ohkoshi, H. Tokoro, T. Matsuda, H. Takahashi, H. Irie, K. Hashimoto, *Angew. Chem.* **2007**, *119*, 3302–3305; *Angew. Chem. Int. Ed.* **2007**, *46*, 3238–3241; b) D.-W. Fu, W. Zhang, H.-L. Cai, Y. Zhang, J.-Z. Ge, R.-G. Xiong, S. D. Huang, N. Takayoshi, *Angew. Chem.* **2011**, *123*, 12153–12157; *Angew. Chem. Int. Ed.* **2011**, *50*, 11947–11951; c) Z. H. Sun, T. L. Chen, J. H. Luo, M. C. Hong, *Angew. Chem.* **2012**, *124*, 3937–3942; *Angew. Chem. Int. Ed.* **2012**, *51*, 3871–3876.
- [3] a) W. Zhang, H.-Y. Ye, H.-L. Cai, J.-Z. Ge, R.-G. Xiong, S. P. D. Huang, *J. Am. Chem. Soc.* **2010**, *132*, 7300–7302; b) G.-C. Xu, W. Zhang, X.-M. Ma, Y.-H. Chen, L. Zhang, H.-L. Cai, Z.-M. Wang, R.-G. Xiong, S. Gao, *J. Am. Chem. Soc.* **2011**, *133*, 14948–14951.
- [4] a) D.-W. Fu, W. Zhang, H.-L. Cai, J.-Z. Ge, Y. Zhang, R.-G. Xiong, *Adv. Mater.* **2011**, *23*, 5658–5662; b) D. W. Fu, H. L. Cai, Y. M. Liu, Q. Ye, W. Zhang, Y. Zhang, X. Y. Chen, G. Giovannetti, M. Capone, J. Y. Li, R. G. Xiong, *Science* **2013**, *339*, 425–428.
- [5] T. Akutagawa, H. Koshinaka, D. Sato, S. Takeda, S.-I. Noro, H. Takahashi, R. Kumai, Y. Tokura, T. Nakamura, *Nat. Mater.* **2009**, *8*, 342–347.
- [6] a) D.-W. Fu, W. Zhang, H.-L. Cai, Y. Zhang, J.-Z. Ge, R.-G. Xiong, S. D. Huang, *J. Am. Chem. Soc.* **2011**, *133*, 12780–12786;

- b) D.-W. Fu, H.-L. Cai, S.-H. Li, Q. Ye, L. Zhou, W. Zhang, Y. Zhang, F. Deng, R.-G. Xiong, *Phys. Rev. Lett.* **2013**, *110*, 257601.
- [7] A. S. Tayi, A. K. Shveyd, A. C.-H. Sue, J. M. Szarko, B. S. Rolczynski, D. Cao, T. Jackson Kennedy, A. A. Sarjeant, C. L. Stern, W. F. Paxton, W. Wu, S. K. Dey, A. C. Fahrenbach, J. R. Guest, H. Mohseni, L. X. Chen, K. L. Wang, J. F. Stoddart, S. I. Stupp, *Nature* **2012**, *488*, 485–489.
- [8] Crystal data for **1** at 293 K: [(C<sub>12</sub>H<sub>20</sub>N)(18C6)](ClO<sub>4</sub>),  $M_r = 542.05$ , orthorhombic, *Ibam*,  $a = 17.083(3)$ ,  $b = 17.615(4)$ ,  $c = 19.139(4)$  Å,  $V = 5759(2)$  Å<sup>3</sup>,  $Z = 8$ ,  $\rho_{\text{calcd}} = 1.25$  Mg m<sup>-3</sup>,  $R_1$  ( $I > 2\sigma(I)$ ) = 0.0790,  $wR_2$  (all data) = 0.2338,  $\mu = 0.184$  mm<sup>-1</sup>,  $S = 1.050$ . **1** at 173 K: orthorhombic, *Pbcn*,  $a = 16.874(4)$ ,  $b = 17.507(4)$ ,  $c = 18.943(5)$  Å,  $V = 5596(2)$  Å<sup>3</sup>,  $Z = 8$ ,  $\rho_{\text{calcd}} = 1.287$  Mg m<sup>-3</sup>,  $R_1$  ( $I > 2\sigma(I)$ ) = 0.0591,  $wR_2$  (all data) = 0.1677,  $\mu = 0.190$  mm<sup>-1</sup>,  $S = 1.158$ . **1** at 93 K: orthorhombic, *Pna2<sub>1</sub>*,  $a = 18.831(4)$ ,  $b = 17.464(3)$ ,  $c = 16.720(3)$  Å,  $V = 5498.6(3)$  Å<sup>3</sup>,  $Z = 8$ ,  $\rho_{\text{calcd}} = 1.310$  Mg m<sup>-3</sup>,  $R_1$  ( $I > 2\sigma(I)$ ) = 0.0374,  $wR_2$  (all data) = 0.1051,  $\mu = 0.193$  mm<sup>-1</sup>,  $S = 1.116$ . XRD patterns at different temperatures are shown in the Supporting Information, Figure S2.
- [9] T. Akutagawa, T. Nakamura, *Dalton Trans.* **2008**, 6335–6345.
- [10] H. D. Flack, *Acta Crystallogr.* **1983**, *A39*, 876–881.
- [11] J. Fousek, V. Janovec, *J. Appl. Phys.* **1969**, *40*, 135–142.
- [12] M. E. Lines, A. M. Glass, *Principles and Applications of Ferroelectrics and Related Materials*, Clarendon, Oxford, **1977**, pp. 94–102.
- [13] G. M. Sheldrick, *Acta Crystallogr.* **2008**, *A64*, 112–122.
- [14] K. Aizu, *Phys. Rev. B* **1970**, *2*, 754–772.
- [15] a) H.-L. Cai, W. Zhang, J.-Z. Ge, Y. Zhang, K. Awaga, T. Nakamura, R.-G. Xiong, *Phys. Rev. Lett.* **2011**, *107*, 147601; b) Y. Zhang, W. Zhang, S.-H. Li, Q. Ye, H.-L. Cai, F. Deng, R.-G. Xiong, S. D. Huang, *J. Am. Chem. Soc.* **2012**, *134*, 11044–11049.
- [16] a) T. Hang, W. Zhang, H.-Y. Ye, R.-G. Xiong, *Chem. Soc. Rev.* **2011**, *40*, 3577–3598; b) W. Zhang, R.-G. Xiong, *Chem. Rev.* **2012**, *112*, 1163–1195.